Cell
PRESS

Structure
Article

The Structural Basis for Unidirectional Rotation of Thermoalkaliphilic F₁-ATPase

Achim Stocker,[1,4] Stefanie Keis,[2] Janet Vonck,[3] Gregory M. Cook,[2] and Peter Dimroth[1,*]
[1] Institute of Microbiology ETH Zürich, ETH Hönggerberg, Wolfgang-Pauli-Strasse 10, CH-8093 Zürich, Switzerland
[2] Department of Microbiology and Immunology, University of Otago, Dunedin 9016, New Zealand
[3] Max-Planck-Institute of Biophysics, Max-von-Laue-Strasse 3, D-60438 Frankfurt, Germany
[4] Present address: Department of Chemistry and Biochemistry, University of Berne, Freiestrasse 3, CH-3012 Berne, Switzerland.
*Correspondence: dimroth@micro.biol.ethz.ch

SUMMARY

The ATP synthase of the thermoalkaliphilic *Bacillus* sp. TA2.A1 operates exclusively in ATP synthesis direction. In the crystal structure of the nucleotide-free $\alpha_3\beta_3\gamma\epsilon$ subcomplex (TA2F₁) at 3.1 Å resolution, all three β subunits adopt the open β_E conformation. The structure shows salt bridges between the helix-turn-helix motif of the C-terminal domain of the β_E subunit (residues Asp372 and Asp375) and the N-terminal helix of the γ subunit (residues Arg9 and Arg10). These electrostatic forces pull the γ shaft out of the rotational center and impede rotation through steric interference with the β_E subunit. Replacement of Arg9 and Arg10 with glutamines eliminates the salt bridges and results in an activation of ATP hydrolysis activity, suggesting that these salt bridges prevent the native enzyme from rotating in ATP hydrolysis direction. A similar bending of the γ shaft as in the TA2F₁ structure was observed by single-particle analysis of the TA2F₁Fₒ holoenzyme.

INTRODUCTION

F₁Fₒ-ATP synthase is a twin rotary engine that reversibly couples ion translocation across the membrane via mechanical rotation to the formation of ATP from ADP and inorganic phosphate (Boyer, 1997; Capaldi and Aggeler, 2002; Dimroth et al., 2006; Noji and Yoshida, 2001). The membrane-embedded Fₒ sector with subunits ab_2c_{10-15} transports the ions, and the cytoplasmic F₁ sector with subunits $\alpha_3\beta_3\gamma\delta\epsilon$ produces the ATP. During either ATP synthesis or hydrolysis, the rotor with subunit composition $\gamma\epsilon c_{10-15}$ rotates against the stator composed of $\alpha_3\beta_3\delta ab_2$.

The bidirectional operation mode of the F₁Fₒ-ATP synthase requires regulation to control the direction of rotation and its velocity. For example, the ATPase activity of mitochondria is tightly regulated by the natural inhibitor protein IF₁, which binds to the ATP synthase at the C-terminal region of the catalytic β subunit (Cabezón et al.,

2003). No homolog of IF₁ has been found in either chloroplasts or bacteria. ATPase activity of the chloroplast F₁Fₒ-ATP synthase (CF₁Fₒ) is also subject to complex regulation to prevent wasteful ATP hydrolysis in the dark. Under such conditions, the enzyme is inhibited by Mg^{2+}-ADP (Digel et al., 1998), conformational transitions of the ε subunit (Nowak and McCarty, 2004; Nowak et al., 2002; Richter et al., 1984), and the oxidation/reduction state of the γ disulfide bond (Nalin and McCarty, 1984). For bacteria, investigations have mainly focused on the role of the ε subunit as a putative inhibitor, coupling factor, or regulator of the ATP synthase (Feniouk et al., 2006; Zimmermann et al., 2005). Depending on the conformation of the ε subunit, the ATP synthase of *Escherichia coli* appears either to be poised in the ATP synthesis direction or to operate in both directions equally well (Gibbons et al., 2000; Rodgers and Wilce, 2000; Tsunoda et al., 2001).

At present, detailed X-ray structural information about F₁ complexes comes from the high-resolution structures of bovine and rat mitochondrial ATPase (Abrahams et al., 1994; Bianchet et al., 1998; Gibbons et al., 2000; Kagawa et al., 2004; Menz et al., 2001). For bacterial F₁ complexes, structural information is limited to the $\alpha_3\beta_3\gamma\epsilon$ complex from *E. coli* resolved at 4.4 Å resolution (Hausrath et al., 1999) and the $\alpha_3\beta_3$ core complex of F₁ from the thermophilic bacterium PS3 at 3.2 Å resolution (Shirakihara et al., 1997). These bacterial F₁-ATPases have the capacity to work in both directions of ATP synthesis and hydrolysis.

A unique feature of F₁Fₒ-ATP synthases from alkaliphilic bacilli is a built-in latency of ATP hydrolysis activity (Cook et al., 2003; Hicks and Krulwich, 1990; Hoffmann and Dimroth, 1990). This inhibition of ATPase activity is most pronounced in the ATP synthase from the thermoalkaliphile *Bacillus* sp. TA2.A1 (TA2F₁Fₒ) and is intrinsic to the F₁ moiety (Cook et al., 2003; Keis et al., 2006). The detergent lauryldimethylamine oxide (LDAO) activates TA2F₁Fₒ-ATPase and TA2F₁-ATPase activity 20- and 30-fold, respectively (Keis et al., 2006). Under LDAO-stimulated conditions, the enzyme is uncoupled, that is, resistant to inhibition by N,N′-dicyclohexylcarbodiimide (Keis et al., 2006). Some of the ATPase inhibition is attributable to the ε subunit, where removal of the C-terminal arm ($\epsilon^{\Delta C}$) results in a 5-fold activation of ATPase activity (Keis et al., 2006). However, the $\epsilon^{\Delta C}$ mutant is still activated 8-fold by LDAO, suggesting that other mechanisms are also

Table 1. X-Ray Structure Determination

Data Collection			
Space group	P2$_1$2$_1$2$_1$		
Cell parameters (Å)			
a, b, c	123.21, 173.02, 218.05		
Resolution range (Å)	50.0–3.06	3.42–3.06	
Total reflections	318,080	82,304	
Unique reflections	81,270	22,103	
I/σ	12.6	2.8	
R$_{merge}$[a]	0.18	0.51	
Completeness (%)	91.4	89.1	
Refinement			
Resolution range (Å)	39–3.06		
Number of work set/test set reflections	93,238/2,390		
R (%)	28.3		
R$_{free}$	31.3		
Number of atoms	29,988		
Rmsd's from ideality			
Bond lengths (Å)	0.008		
Bond angles (°)	1.2		
B factors (Å^2)	Average	Minimum	Maximum
α	93.1	39.8	283.4
β	86.7	40.3	324.9
γ	60.9	2.2	176.6
ε	108.4	31.4	249.3

[a] $R_{merge} = (\sum_h \sum_j |I_j(h) - <I_{(h)}>|)/(\sum_h \sum_j I_j(h))$, where $I_j(h)$ is the jth measurement of the intensity of reflection h and $<I_{(h)}>$ is the mean intensity of equivalent reflections.

operating to block ATP hydrolysis activity. To gain further insight into the structural basis of inhibition of the ATP hydrolysis activity, we initiated studies to crystallize the F_1 moiety of the TA2F$_1$F$_o$-ATP synthase (Stocker et al., 2005).

In this communication, we present the structure of TA2F$_1$ (lacking the δ subunit) at 3.1 Å resolution. The structure was obtained in the absence of magnesium and nucleotides. Under these conditions, a pseudo three-fold noncrystallographic symmetry axis relates the three α and β subunits. Despite the noncrystallographic symmetry relation, and the fact that subunits γ and ε are only present as single copies in the complex, major portions of both are clearly resolved, allowing structural features to be revealed in atomic detail. The data show that the asymmetrical γ stalk of the rotor is distorted within the cavity of the $\alpha_3\beta_3$ cylinder, thereby preventing rotation in the ATP hydrolysis direction due to steric interference with the catalytic β subunit. A similar distortion of the γ stalk is seen in electron micrographs of the TA2F$_1$F$_o$-ATP synthase complex, indicating that this is not an artifact of the isolated TA2F$_1$ subcomplex.

RESULTS

Structure Determination and Map Interpretation

Crystals of the nucleotide-free subcomplex of TA2F$_1$, lacking the δ subunit, were obtained as described previously (Stocker et al., 2005). A complete data set diffracting to 3.1 Å was obtained from one single crystal (Table 1). The structure of TA2F$_1$ was determined by molecular replacement using the structural model of bovine heart mitochondrial F$_1$ (Abrahams et al., 1994), which contains one catalytic subunit in the open β_E conformation with no bound nucleotide. In the refinement of the model, all β subunits were converted into the β_E conformation (see Experimental Procedures). Subsequently, the γ and ε subunits were built into the electron density map. The asymmetric unit in our crystal contains one single TA2F$_1$ molecule with $\alpha_3\beta_3\gamma\varepsilon$ subunit stoichiometry. A noncrystallographic three-fold symmetry axis relates the $\alpha\beta$ sectors within the $\alpha_3\beta_3$ hexamer of TA2F$_1$. With the exception of one localized region in the α subunit (residues 393–406), the electron density of the α and β subunits was well defined. As a consequence of the noncrystallographic three-fold symmetry, interpretable
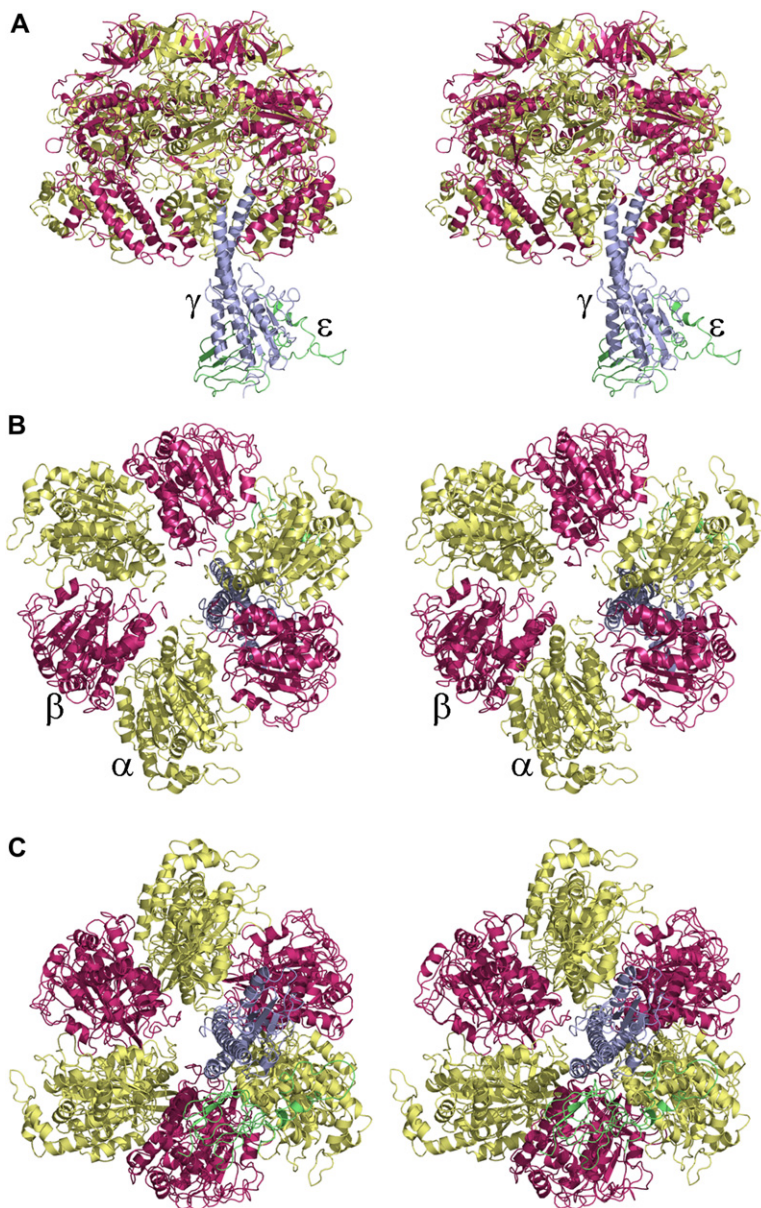
Figure 1. Stereo Drawings of the Three-Dimensional Structure of the $\alpha_3\beta_3\gamma\epsilon$ Subcomplex of F$_1$ from the Thermoalkaliphilic *Bacillus* sp. TA2.A1

(A) Side view of the complex with the pseudo three-fold axis vertical. Three structural domains are visible in each subunit of the $\alpha_3\beta_3$ hexamer. The β and α subunits are shown in pink and pale yellow, respectively. The γ subunit and the ϵ subunit with the highest occupancy are shown in light blue and lime, respectively.

(B) Top view of the complex viewed toward the membrane; the pseudo three-fold axis points toward the viewer.

(C) Bottom view of the complex viewed from the membrane.

electron density was obtained in three orientations for the asymmetric part of the molecule represented by subunits γ and ϵ. By using the information available from two *E. coli* models (Protein Data Bank [PDB] ID codes 1JNV and 1BSN), major parts of subunits γ and ϵ were built for each orientation. The final TA2F$_1$ model contains a total of 3891 residues including residues 27–500 of the α subunit, residues 2–462 of the β subunit, residues 3–266 of the γ subunit, and residues 1–135 of the ϵ subunit, with a lack of interpretable density for residues 50–63 and 194–216 for the γ subunit. The TA2F$_1$ electron density map was sufficiently well defined to reliably place in it the ϵ subunit.

Overall Molecular Architecture of TA2F$_1$

The symmetric part of the TA2F$_1$ model consists of three α and three β subunits placed alternately around the pseudo

three-fold axis. Subunits γ and ϵ represent the asymmetric central stalk, and at the foot of the structure form the interface connecting the catalytic F$_1$ head group with the membrane-embedded F$_o$ sector in the native F$_1$F$_o$-ATP synthase (Figure 1A).

The α and β subunits of TA2F$_1$ have a similar overall fold as recognized in previous F$_1$ structures (Abrahams et al., 1994; Shirakihara et al., 1997). However, all six nucleotide-binding sites in the TA2F$_1$ structure are unoccupied, as expected from the isolation procedure in the absence of nucleotides and magnesium. Therefore, the three catalytic β subunits are all in an open site conformation and denoted β_E in accordance with the annotation of the reference structure (Abrahams et al., 1994). As a consequence, the $\alpha_3\beta_3$ core complex in TA2F$_1$ adopts a highly symmetrical overall conformation which is essentially identical to

the $\alpha_3\beta_3$ structure of the moderately thermophilic *Bacillus* PS3 (Shirakihara et al., 1997). Accordingly, the $C\alpha$ atoms of the PS3 $\alpha\beta$ assembly superimpose with root-mean-square deviations (rmsds) of 1.11, 1.16, and 1.05 Å with the corresponding TA2 $\alpha\beta$ assemblies. The overall superposition of the two $\alpha_3\beta_3$ assemblies yields an rmsd for the $C\alpha$ atoms of 1.07 Å. At the top of the TA2 $\alpha_3\beta_3$ assembly, the N-terminal β barrel domains from the α and β subunits form a relatively narrow crown with pseudo three-fold symmetry (Figure 1B). The $C\alpha$ atoms of the three TA2 $\alpha\beta$ assemblies superimpose with rmsds of 0.66, 0.70, and 0.73 Å, respectively. The $C\alpha$ atoms of the three α subunits superimpose with rmsds of 0.59, 0.59, and 0.60 Å, respectively, and for the three β subunits superimpose with rmsds of 0.55, 0.47, and 0.52 Å, respectively. Further down, a large internal cavity opens due to a large hinge motion of the C-terminal part in the catalytic β subunits (Figure 1C). These regions are rotated away from the central axis by about 11° (Figure 1A). The pseudo three-fold symmetry of the cavity breaks down in this region because the helical shaft of the γ subunit is inserted asymmetrically into the $\alpha_3\beta_3$ core complex, with the N-terminal α helix being in close contact only with one of the three β_E subunits.

At the bottom of the helical stalk region, the γ subunit has a more globular protrusion on one side. On the opposite side, the γ subunit interfaces with the ϵ subunit, of which mainly its N-terminal ten-stranded β barrel is visible.

Structural Features of the γ Subunit

The γ subunit in TA2F_1 encompasses residues 3–266 and adopts a similar overall fold as its *E. coli* counterpart (Hausrath et al., 1999, 2001; Rodgers and Wilce, 2000). Accordingly, the γ subunits of TA2F_1 and of *E. coli* F_1 superimpose with an rmsd for the $C\alpha$ atoms of 1.52 Å (Figure 2A). Figure 2B shows a comparison of the relative positions of the γ subunits within the F_1 complexes originating from yeast, bovine mitochondria, *E. coli*, and TA2F_1. In the first three structures, the lower part of the C-terminal helix of the γ stalk coincides with the rotational axis of the motor. In the TA2F_1 structure, however, the corresponding part of the γ stalk is tilted by approximately 11° against the putative rotational center (Figures 2B and 2C).

The TA2F_1 γ stalk is composed of the N-terminal α helix (residues 3–64) and the C-terminal α helix (residues 211–266). The two helices are positioned such that the N-terminal helix faces exclusively one single β_E subunit at its C-terminal helix-turn-helix motif (residues 353–405) with the C-terminal helix of the γ subunit coiling around the N-terminal helix. The molecular details of the interaction between the N-terminal α helix of the γ shaft and the helix-turn-helix motif of the β_E subunit are depicted in Figure 3. The N terminus of the γ subunit contains a cluster of four positively charged side chains (Lys8, Arg9, Arg10, and Arg12), of which Arg9 and Arg10 are directly involved in the formation of two adjacent salt bridges toward the negatively charged side chains Asp372 and Asp375 located on helix 2 of the helix-turn-helix motif of the β_E subunit. Sequence alignments of the γ subunit in this region indicate that the local formation of two adjacent salt

bridges is a unique feature of the TA2F_1-ATPase and some closely related bacterial species (see the Supplemental Data available with this article online).

Mechanical Coupling and Mechanistic Implications

The overall function of the asymmetric γ shaft within the F_1 head group is to transmit torque into changing nucleotide affinities of the catalytic sites during ATP synthesis by driving the β subunits through a cycle of hinge-bending motions (Gao et al., 2005; Xing et al., 2005). In this context, our TA2F_1 model may be described as a postsynthesis, postproduct release state, where the γ subunit adopts a unique, inhibitory position within the F_1 head group. Figure 3 highlights the regulatory role of the two salt bridges in maintaining the ATP hydrolysis blocked state of the enzyme by bending the γ subunit toward the helix-turn-helix motif of one β_E subunit. The tight contact between these two subunits is further enforced by the high packing density of adjacent hydrophobic residues (data not shown).

In order to analyze the influence of the positively charged cluster (viz. Lys8, Arg9, Arg10, and Arg12) on ATP hydrolysis activity, we substituted the ^{8}KRRIR^{12} residues of the N terminus of the γ subunit in TA2F_1 to ^{8}QQQIQ^{12} residues (TA2F_1[γ^{4Q}]). SDS-PAGE analysis revealed indistinguishable subunit stoichiometry (Figure 4A). Whereas the TA2F_1 wild-type (WT) enzyme exhibited only marginal ATP hydrolysis activities (0.3 U/mg protein; in the absence of LDAO), the TA2F_1(γ^{4Q}) mutant was a highly active ATPase exhibiting activities of 10 U/mg protein under otherwise identical conditions (Figures 4B and 4C). Hence, the two salt bridges between the positively charged cluster on the γ subunit and the aspartic acids on the helix-turn-helix motif on the β subunit appear to be the structural basis for the inhibition of ATP hydrolysis activity.

It has been well documented that TA2F_1 (WT) exhibits latent ATP hydrolysis activity that can be unmasked in the presence of LDAO (Cook et al., 2003), and indeed, addition of 0.4% LDAO dramatically increased the ATP hydrolysis activity of the wild-type enzyme to 14.1 U/mg protein. In contrast, LDAO addition did not increase the ATP hydrolysis activity of the mutant enzyme but was slightly inhibitory instead (Figures 4B and 4C). The mechanism for unmasking latent ATP hydrolysis activity by LDAO is presently not known in detail, although several observations have been reported (Hicks and Krulwich, 1990; Hoffmann and Dimroth, 1990; Cook et al., 2003; Keis et al., 2004), but the observed differences between wild-type and mutant enzymes suggest that LDAO in some way affects the formation of (strong) salt bridges between γ and β subunits.

Single-Particle Analysis

We have shown that crystals of TA2F_1 possess latent ATP hydrolytic activity (Stocker et al., 2005) indistinguishable from both purified wild-type F_1F_o-ATP synthase and inverted strain TA2.A1 membrane vesicles (Cook et al., 2003). This result led us to address the question of
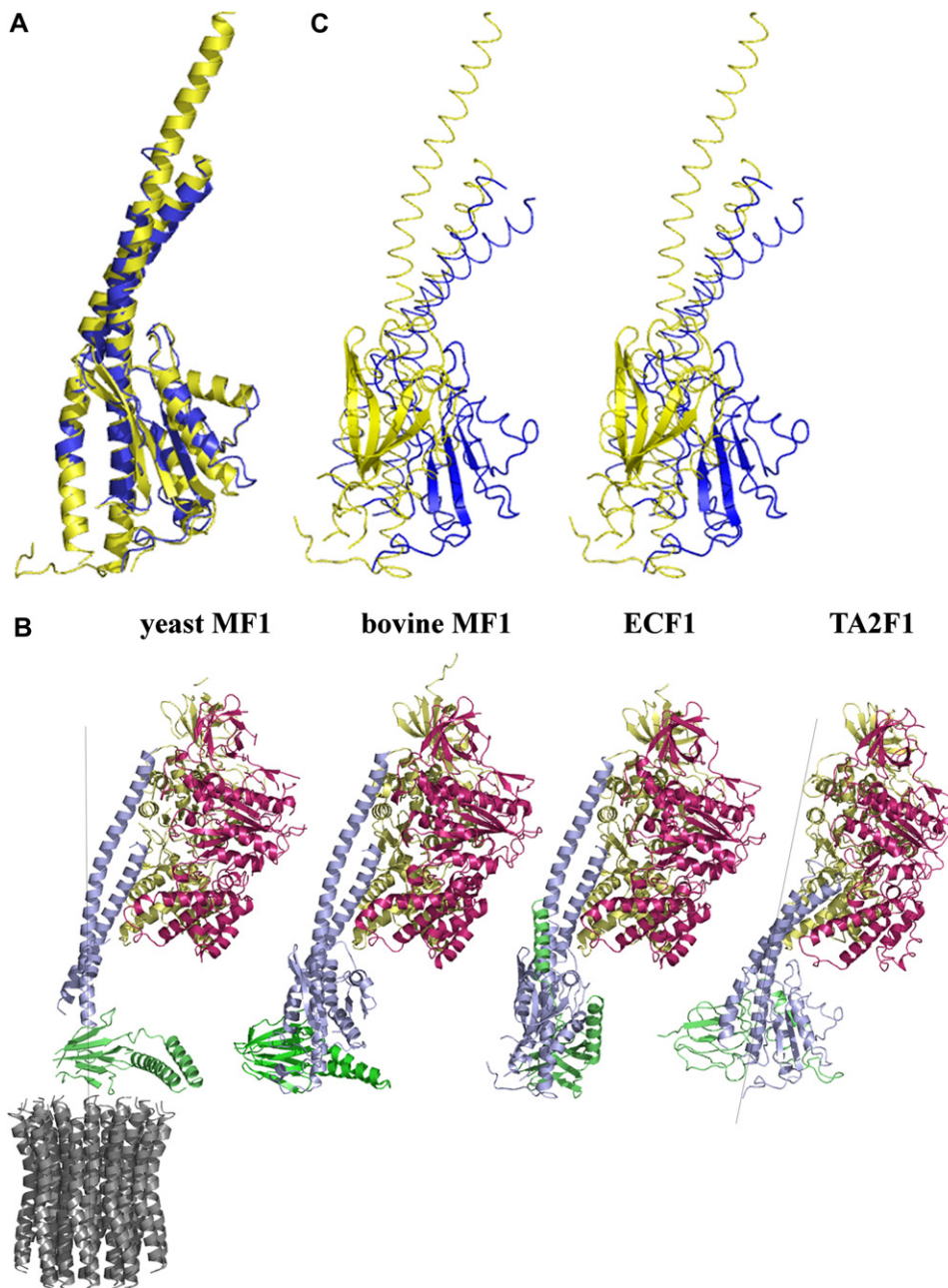
**Figure 2. Conformational Properties and Positional Analysis of γ Subunits within F$_1$ Complexes**

(A) Three-dimensional overlay of the γ subunits of *E. coli* (yellow) and *Bacillus* sp. TA2.A1 (light blue). The overall conformations of the two subunits are very similar and superimpose with an rmsd for the Cα atoms of 1.52 Å.

(B) Relative positions of the γ subunits within the F$_1$ complexes from yeast, bovine mitochondria, *E. coli*, and *Bacillus* sp. TA2.A1. Shown are corresponding $\alpha\beta\gamma\varepsilon$ subcomplexes. The positions of the γ subunits were determined by superposing corresponding α subunits onto the α subunit of the yeast mitochondria F$_1$F$_o$ model. The distortion of the stator-rotor interface in the case of TA2F$_1$ involves a rigid-body bending movement of the γ subunit out of its putative rotational axis.

(C) Stereo drawing of the bent position of the γ subunit within TA2F$_1$ (blue) relative to the position of the γ subunit within ECF$_1$ (yellow).

whether our TA2F$_1$ X-ray structural model may represent the equivalent of the latent state of the TA2F$_1$F$_o$ complex in vivo and thus would aid in understanding the observed adaptive processes within thermoalkaliphilic bacteria. Therefore, electron micrographs of single particles of the purified native TA2F$_1$F$_o$ complex were analyzed (Figure 5A). TA2F$_1$F$_o$ has only two clearly distinguishable views, shown in the class averages of Figure 5B. The majority of particles (Figure 5B, classes 1–4) are characterized by a distinctively bent central stalk, originating near
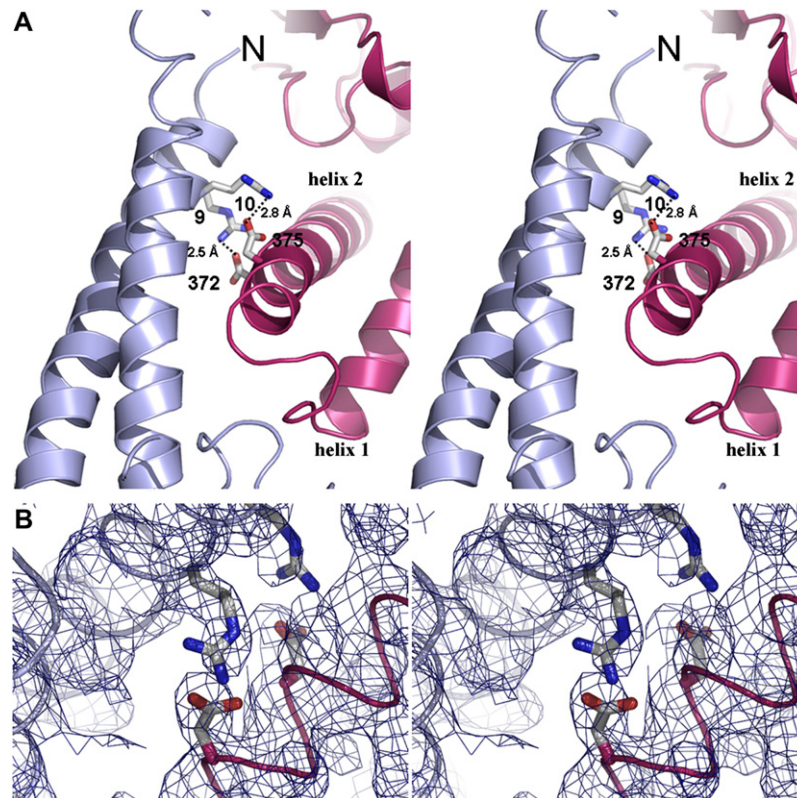
Figure 3. Analysis of Rotor-Stator Interactions within Recombinant TA2F₁

(A) Stereo drawing of the rotor-stator interface of thermoalkaliphilic TA2F₁ depicting two salt bridges between the γ subunit N terminus (residues Arg9 and Arg10) and the helix-turn-helix motif in the β_E subunit (residues Asp372 and Asp375).

(B) Close-up with electron density. Shown is a $2F_o - F_c$ density map contoured at 1.0σ above the mean.

the center of the α₃β₃ head but attached to the far left-hand side of F_o. The F_o complex has a distinct structure, with the c ring visible as a symmetrical U-shaped feature which has the central stalk attached to its left leg. A less distinct extension on the right-hand side of the c ring can be interpreted as the a subunit. The head also has a clear substructure in which the different domains from the X-ray structure can easily be recognized. In addition, the δ sub-unit is visible as a knob on the right-hand side of the α₃β₃ head. The orientation of the stalk (rotor) relative to the sta-tor (a and δ subunits) is fixed, indicating a fixed resting position of the motor. About 35% of the particles (Figure 5B, classes 5–7) show a different view, with a centrally positioned stalk, one central knob on the α₃β₃ head, and a narrower U-shaped F_o domain without indication of an a subunit. This view would represent an orientation of the complex rotated ∼90° relative to the dominant view with the a subunit in the direction of view. The positioning of the central stalk at the edge of the c ring implicates a bend of the γ subunit as seen in the TA2F₁ crystal struc-ture. In order to compare the electron micrograph projec-tions to the TA2F₁ X-ray model, the latter was rotated by hand to give the best fit to the projections using the pro-gram Chimera (Pettersen et al., 2004). As expected, the best fits to the two distinct electron micrograph views

were found to be ∼90° rotated relative to each other, as shown in Figure 5C. The close correspondence indicates that the conformation of the γ subunit is the same in the complete F_1F_o as in the F_1 crystal.

DISCUSSION

Characteristics of Latent ATP Hydrolysis in Alkaliphilic Bacteria

A notable feature of alkaliphilic F_1F_o-ATP synthases is their specific blockage of ATP hydrolysis activity (Cook et al., 2003; Hicks and Krulwich, 1990; Hoffmann and Dim-roth, 1990). This characteristic is most pronounced in the ATP synthase from *Bacillus* sp. TA2.A1 where even after reconstitution into proteoliposomes, ATP-driven proton transport or proton-coupled ATP hydrolysis activity could not be detected (Cook et al., 2003). This blockage is less stringent in the ATP synthases from *Bacillus alcalophilus* and *Bacillus pseudofirmus* OF4, where low but measurable ATP hydrolysis activities coupled to proton transport have been measured (Hicks and Krulwich, 1990; Hoffmann and Dimroth, 1990). We have hypothesized that this unusual property of the TA2F₁F_o-ATP synthase may be a necessity to survive at alkaline pH and high temperature. The en-zyme would neither pump protons outward, thereby
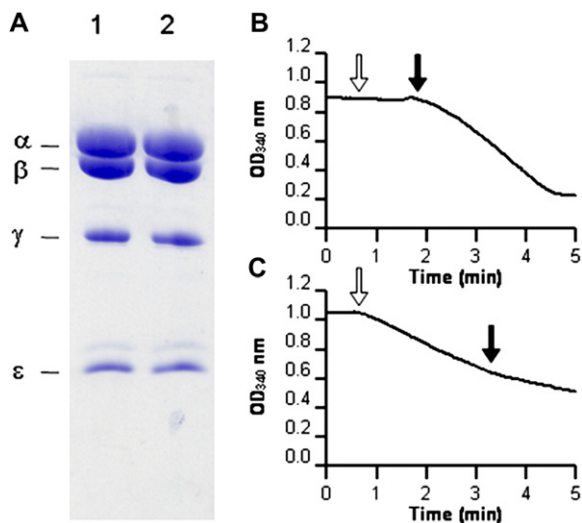
Figure 4. Biochemical Analysis of Recombinant TA2F$_1$

(A) SDS-PAGE of recombinant TA2F$_1$ complexes from the thermoalkaliphilic *Bacillus* sp. TA2.A1. Lane 1, TA2F$_1$(γ^{WT}) (30 μg); lane 2, TA2F$_1$(γ^{4Q}) (30 μg). Samples were resolved by 12% SDS-polyacrylamide gel electrophoresis by the method of Schägger et al. (1988).

(B and C) Effect of LDAO on the ATPase activity of recombinant TA2F$_1$ complexes. ATP hydrolysis of TA2F$_1$(γ^{WT}) (B) and TA2F$_1$(γ^{4Q}) (C) was measured with the ATP-regenerating assay, as described in Experimental Procedures, by monitoring the continuous change in absorbance at 340 nm (OD$_{340}$). The reaction was initiated by the addition of ATP (open arrows). The velocity increase (indicated by arrow) was due to addition of 0.4% (w/v; final concentration) LDAO (filled arrows). Specific activities for TA2F$_1$(γ^{WT}) of 0.31 and of 14.09 U/mg and for TA2F$_1$(γ^{4Q}) of 10.01 and of 4.91 U/mg in the absence and presence of LDAO, respectively, were observed.

raising the internal pH to potentially intolerable values, nor would it waste intracellular ATP at potentially low proton motive force values, impeding survival in the alkaline environment (Dimroth and Cook, 2004). When measuring latent hydrolysis of TA2F$_1$ in the ATP-regenerating assay at high ATP concentrations (>2 mM), a slow but steady release of latency is observed (unpublished data). This finding supports the notion that the blockage of ATP hydrolysis in TA2F$_1$ is released by high substrate (Mg^{2+}-ATP) concentrations. This process of self-activation implies that in part of the TA2F$_1$ molecules, the inhibition is relieved through the binding of Mg^{2+}-ATP and a concomitant conformational change of the corresponding β subunit. Conversely, nucleotide depletion elicits an opposite conformational change in the β subunit, which causes stringent blockage of ATPase activity within TA2F$_1$.

The Molecular Basis of γ-Mediated Latent ATP Hydrolysis

Several crystal structures of F$_1$-ATPases have been reported in which the asymmetric γ shaft has a distinct position within the α$_3$β$_3$ core complex in accordance with the current view of F$_1$ function (Braig et al., 2000; Menz et al., 2001). In these structures, a cluster of positively charged residues represents a circular track on the surface of the
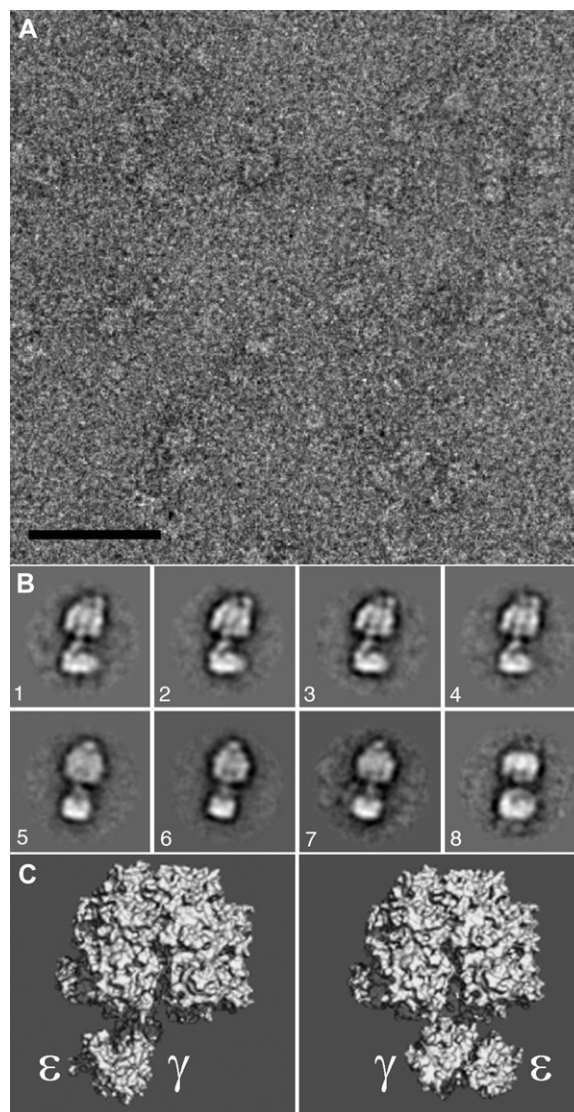
Figure 5. Electron Microscopic Analysis of Native TA2F$_1$F$_o$

(A) Electron micrograph of TA2F$_1$F$_o$ negatively stained with uranyl acetate. The scale bar represents 50 nm.

(B) Class averages after multivariate statistical analysis and classification of 1940 particles. At least 20% of particles were rejected based on poor resolution, as well as 20% from each class. Classes 1–8 contain 197, 250, 197, 194, 184, 261, 141, and 129 particles, respectively. Classes 1–4 show a view with the central stalk attached asymmetrically on the left side of the *c* ring; classes 5–7 show a more centrally connected stalk and a much narrower F$_o$ domain. Class 8 contains some poorly aligned particles, of which some have the F$_1$ domain facing down. Each frame represents 382 Å.

(C) Corresponding views of the TA2F$_1$ structure rotated approximately 90° relative to each other. The images were created using UCSF Chimera (Pettersen et al., 2004).

γ shaft which guides the hinge movements of the catalytic β subunits. Theoretical and experimental studies indicate that the annealing of nucleotides drives the rotation of the γ stalk by steric and electrostatic interactions (Itoh et al., 2004; Lowry and Frasch, 2005; Xing et al., 2005;

Yasuda et al., 2001). In the ATP hydrolytic cycle, two catalytic β subunits are mechanically coupled: the binding of substrate (Mg^{2+}-ATP) induces an inward hinge-bending motion of the respective β subunit and a synchronous outward movement of the adjacent β subunit with a concomitant release of ADP and phosphate (Menz et al., 2001). In contrast to these F$_1$ complexes, which are catalytically active ATPases, the TA2F$_1$ complex has latent ATP hydrolytic activity. It is important to note that in the TA2F$_1$F$_o$-ATP synthase preparation as well as in the TA2F$_1$-ATPase crystals used for structure determination by electron microscopy and X-ray diffraction, respectively, the latent ATP hydrolysis activity was retained. To our knowledge, the present structures represent the first ATP synthase conformations that are unable to hydrolyze ATP and thus provide insights into the mechanism of this blockage.

In the reported structures of ATPases that hydrolyze ATP, the C-terminal α helix of the γ shaft extends continuously throughout the central cavity of the α$_3$β$_3$ core complex (Hausrath et al., 2001; Rodgers and Wilce, 2000; Stock et al., 1999). In these F$_1$ complexes, the N-terminal β barrel domains from the α and β subunits form a bearing into which the C-terminal γ stalk extends. In the TA2F$_1$ structure, however, the upper third of the γ stalk (residues 267–286) has no interpretable density. Neither SDS-PAGE analysis of the crystals nor mass spectrometry of soluble TA2F$_1$ revealed any evidence for degradation of the γ subunit (Cook et al., 2003; Stocker et al., 2005). These data suggest that the C-terminal helix of the γ subunit above residue 266 is disordered.

In the present TA2F$_1$ structure, the visible part of the γ subunit is shifted by a bending movement toward a single β$_E$ subunit (Figures 2A–2C). This conformation causes a close contact between the γ and this β subunit which prevents rotation. Two salt bridges stabilize this conformation and trap the γ subunit in this position. The fundamental role of these salt bridges in blocking rotation is confirmed by biochemical evidence showing that mutations of the amino acids involved in salt-bridge formation releases the latent ATP hydrolysis activity (Figure 4). This conclusion is also in accord with results from sequence alignments of the γ subunit showing that TA2F$_1$ has an unusually high number of salt bridges between γ and β in this region (see the Supplemental Data). In addition, these alignments indicate that the potential formation of a similar steric blockage within mitochondrial F$_1$-ATPases is not likely to occur due to the absence of a negatively charged amino acid side chain corresponding to Asp372 of TA2F$_1$-ATPase.

Even in the absence of a TA2F$_1$ structure with bound nucleotides, we propose that the crucial steric interaction between the γ and a β$_E$ subunit that provides the basis for latent ATP hydrolysis activity would not be affected by conformational changes elicited by nucleotide binding to the other β subunits. This hypothesis is in agreement with biochemical evidence showing that the enzyme is unable to hydrolyze ATP under conditions where nucleotides are expected to be bound, but is still competent for ATP synthesis (Cook et al., 2003). On the basis of these observations, we conclude that the escape route of TA2F$_1$ from

its blocked state involves torque generation by the F$_o$ motor and ATP synthesis.

Is the TA2F$_1$ Structural Model Representative for TA2F$_1$F$_o$?

To answer the question of whether the unusual γ subunit conformation in TA2F$_1$ is relevant for the whole complex, we have studied TA2F$_1$F$_o$ by electron microscopy. The particles displayed very clear subunit structure and the majority of these particles were oriented with the δ and a subunits on the right-hand side of the complex and the central stalk attached to the left-hand side of the c ring. The bent conformation of the central stalk is different from the negative stain 3D reconstruction of EF$_1$F$_o$ (Böttcher et al., 2000) and the cryoelectron microscopy reconstructions of CF$_1$F$_o$ (Mellwig and Böttcher, 2003) and bovine heart mitochondrial F$_1$F$_o$ (Rubinstein et al., 2003). In these three enzymes, the central stalk is not bent. Therefore, the TA2F$_1$F$_o$ shows the same conformational feature of the γ stalk as is observed in TA2F$_1$, demonstrating that this is not an artifact of crystallization. A similar configuration of the central stalk was observed recently in electron micrographs of the F$_1$F$_0$ ATP synthase from the hyperthermophilic bacterium *Aquifex aeolicus* (Peng et al., 2006). We propose that the dominant orientation of the enzyme represents a unique resting conformation of the rotor versus the stator in its latent ATP hydrolysis state and that this resembles the resting state that has been observed in the CF$_1$F$_o$, another enzyme that exhibits latent ATP hydrolysis activity (Mellwig and Böttcher, 2003).

EXPERIMENTAL PROCEDURES

Bacterial Strains

E. coli DH10B (Hanahan et al., 1991) was used for all cloning experiments, and *E. coli* RNE41(DE3) (a gift from B. Miroux, Meudon, France) was used to overproduce the TA2F$_1$ complexes from the ATP synthase of *Bacillus* sp. TA2.A1.

Construction of Expression Plasmids

The construction of the expression plasmid pTrcα-ε, containing all of the F$_1$ genes except for *atpH*, has been described previously (Stocker et al., 2005). To construct a γ mutant plasmid, the [8]KRRIR[12] residues in the γ subunit of pTrcα-ε were substituted with [8]QQQIQ[12] residues by the overlap extension PCR method (Ho et al., 1989) as follows. Two pairs of primers, TA2atpAfwd (5′-GCATCAGACCTGAAGAAATC-3′) with atpGrev2 (5′-CGActGGATctGCtGTTgAATCTCTCTCATTCCTTG-3′) and atpGfwd2 (5′-ATTcAACaGGCagATCCagTCGGTAAAAAATAC ACGC-3) with B9SEQ1 (5′-CAGGGTCAAGGTTTCAAGCA-3′), were used to generate mutated DNA fragments, where lowercase nucleotides indicate the specific changes in a primer for site-directed mutagenesis. These fragments, which overlapped by 21 nucleotides, were subsequently used for overlap extension PCR with the external primers TA2atpAfwd and B9SEQ1. The amplified product obtained was then digested with BglII and SspI. This 1.7 kb BglII-SspI fragment was simultaneously cloned with a 2.3 kb SspI-ClaI fragment from pTA2F$_1$ (Stocker et al., 2005) into pTrcα-ε digested with BglII and ClaI. The new plasmid was designated pγ4Q and the region amplified by PCR was confirmed by DNA sequencing.

Expression and Purification of Recombinant TA2F$_1$ Complexes

Expression of the plasmids pTrcα-ε and pγ4Q (TA2F$_1$[γ^{4Q}]) in *E. coli* RNE41(DE3) and purification of TA2F$_1$ complexes was accomplished

as described previously (Stocker et al., 2005). Purified TA2F$_1$ complexes were immediately used for crystallization trials. The progress of the purification was monitored by comparing the latent and LDAO-stimulated ATP hydrolysis activity with the ATP-regenerating assay.

Crystallization and Data Collection

Protein (6 mg/ml) in 20 mM Tris-HCl (pH 8.0), 100 mM NaCl, 1 mM EDTA, and reservoir buffer containing 1 M LiCl, 100 mM Tris-HCl (pH 8.8), and 20% (w/v) polyethylene glycol (PEG) 6000 was mixed 1:1 to yield a final volume of 4 µl in 70 µl of dry paraffin oil. TA2F$_1$ crystals with dimensions 0.15 × 0.15 × 0.3 mm and well-defined edges and faces were selected after 2 days of growth at 23°C. The selected crystals were transferred for 10 min into mother liquor with increasing concentrations of PEG 400 in four steps from 5% to 20% (w/v) and flash-frozen in liquid nitrogen. Complete X-ray diffraction data sets were collected from single crystals at the SLS PX beamline at the Paul Scherrer Institute in Villigen, Switzerland. Indexing, integration, scaling, postrefinement, and reduction of the data were carried out using the XDS package (Kabsch, 1993).

Structure Determination and Refinement

The structure was solved by molecular replacement using the program Phaser (McCoy et al., 2005). The atomic coordinates derived from the refined structural model of bovine mitochondrial F$_1$ (Abrahams et al., 1994) were used as a search model in the calculation. Three prominent solutions with high log (likelihood) gain and high translation function Z score were obtained (McCoy et al., 2005). In all subsequent refinement steps, 2.5% of the data was set aside for calculation of the free R factor. Initial rigid-body refinements using the CNS software suite (Brünger et al., 1998) indicated that two of the three β subunits in our model differed significantly from the initial search model. Replacement of these β subunits by nucleotide-free β$_E$ subunits brought about a further decrease of the free R factor by 4%. Subunits were labeled according to the F$_1$ reference structure from bovine heart mitochondria (Abrahams et al., 1994). Subsequently, the α$_3$β$_3$ core of our model was mutated to the TA2F$_1$ sequence using the program Coot (Emsley and Cowtan, 2004). According to the structure of mitochondrial F$_1$, three domains in α (residues 27–95; 96–384; 385–500) and in β (residues 2–111; 112–318; 319–462) were defined for further rigid-body minimization. Subsequently, restrained refinement including TLS refinement (Winn et al., 2001) was performed using the program REFMAC (CCP4, 1994) as well as the PHENIX program suite (Adams et al., 2004). Noncrystallographic symmetry restraints were defined automatically for the α and β subunits using PHENIX. The model was revised at each cycle of the refinement by inspection of the F$_o$ − F$_c$ and 2F$_o$ − F$_c$ maps and manual rebuilding in Coot. At this point, it became possible to model new features in the central stalk, initially as polyalanine chains. Residues 3–49 and 217–266 corresponding to the N- and C-terminal helices of the γ subunit were built into the density using the structure of the equivalent *E. coli* γ subunit (PDB ID code 1JNV). During subsequent refinement, it became clear that electron density was visible for two more γ subunits. We interpret this as alternating conformations of the central stalk region which occupy three positions. Consequently, three alternating conformations (A, B, and C) of the γ and ε subunits were modeled and refined at occupancies of 20%, 35%, and 45%, respectively. Figures were produced using the program PyMOL (DeLano, 2002). Statistics are given in Table 1.

Purification of TA2F$_1$F$_o$-ATP Synthase for Electron Microscopy

Cells of *Bacillus* sp. TA2.A1 (200 g wet weight) were resuspended in 200 ml of 50 mM Tris-HCl (pH 8.0) containing 15 mM MgCl$_2$, 1 mM DTT, and 0.1 mM diisopropylfluorophosphate (DFP). DNaseI and lysozyme were added to a final concentration of 0.2 and 2.4 mg/ml, respectively, and the suspension was stirred for 1 hr at 37°C. After homogenization with a glass teflon pestle, protoplasts were broken by two passages through a French pressure cell at 82 Mpa, and debris was removed by centrifugation at 15,000 × g for 30 min. The supernatant was centrifuged for 3 hr at 200,000 × g and the harvested membrane vesicles were resuspended in 30 ml of resuspension buffer (50 mM Tris-HCl [pH 8.0], 50 mM Na$_2$SO$_4$, 2 mM MgCl$_2$, 1 mM DTT, 0.1 mM DFP, and 10% glycerol) containing 2% sodium cholate. The suspension was gently stirred on ice for 30 min and then centrifuged for 1 hr at 200,000 × g. To extract TA2F$_1$F$_o$ from the cytoplasmic membrane, membrane vesicles were resuspended in resuspension buffer containing 2% β-dodecylmaltoside and gently stirred for 1 hr at 25°C. Nonsolubilized material was removed by ultracentrifugation at 120,000 × g for 3 hr and the red supernatant was diluted by one third of its volume with 80 mM Tris-HCl (pH 8.0) containing 2 M NaCl, 20 mM MgCl$_2$, and 40% glycerol. The supernatant was loaded onto a 50 ml column of chelating Sepharose Fast Flow (Amersham Biosciences) previously loaded with CuSO$_4$ and equilibrated in five column volumes of 20 mM Tris-HCl (pH 8.0) containing 0.5 M NaCl, 5 mM MgCl$_2$, 10% glycerol, and 0.02% β-dodecylmaltoside. All further steps of the purification procedure were identical to those described for the purification of recombinant TA2F$_1$ complexes with the exception that 0.02% β-dodecylmaltoside was included in all buffers.

Electron Microscopy and Image Analysis

The F$_1$F$_o$ complexes were negatively stained with 1% (w/v) uranyl acetate. Electron micrographs were collected using a Philips CM120 at 120 kV under low-dose conditions, at a magnification of 44,000× on Kodak SO-163 electron image film. Negatives checked by optical diffraction for correct defocus and lack of drift and astigmatism were digitized on a PhotoScan scanner (Z/I Imaging, Aalen, Germany) at a pixel size of 7 µm. Subsequently, adjacent pixels were averaged to yield a pixel size on the specimen of 4.77 Å. Selection of 1940 particles was made from 30 micrographs using the boxer program from EMAN (Ludtke et al., 1999). Images were processed using IMAGIC V (van Heel et al., 1996). The images were band pass filtered, aligned translationally and rotationally, and subjected to multivariate statistical analysis and classification. Images assigned to the same class were averaged.

Biochemical Methods

Protein concentrations were determined by using the bicinchoninic acid (BCA) protein assay kit from Sigma, with bovine serum albumin as the standard. Purified TA2F$_1$ complexes were analyzed by 12% polyacrylamide gel electrophoresis in the presence of 0.1% SDS (Schägger et al., 1988), and protein bands were visualized by staining with Coomassie brilliant blue. ATP hydrolysis activity was measured at 24°C by using an ATP-regenerating assay. The assay mixture contained 100 mM MOPS (pH 7.5), 3 mM phosphoenolpyruvate, 2 mM MgCl$_2$, 0.25 mM NADH, 0.57 U/ml pyruvate kinase, 3.2 U/ml lactate dehydrogenase, and the indicated concentration of ATP. The reaction was initiated by the addition of ATP to the assay mixture, and the rate of NADH oxidation was monitored continuously at 340 nm. Nine micrograms of TA2F$_1$ subunit complexes was used for measurements. The activity that hydrolyzed 1 µmol of ATP per min is defined as 1 unit.

Supplemental Data

Supplemental Data include sequence alignments and can be found with this article online at http://www.structure.org/cgi/content/full/15/8/904/DC1/.

REFERENCES

Abrahams, J.P., Leslie, A.G.W., Lutter, R., and Walker, J.E. (1994). Structure at 2.8 Å resolution of F$_1$-ATPase from bovine heart mitochondria. Nature *370*, 621–628.

Adams, P.D., Gopal, K., Grosse-Kunstleve, R.W., Hung, L.W., Ioerger, T.R., McCoy, A.J., Moriarty, N.W., Pai, R.K., Read, R.J., Romo, T.D., et al. (2004). Recent developments in the PHENIX software for automated crystallographic structure determination. J. Synchrotron Radiat. *11*, 53–55.

Bianchet, M.A., Hullihen, J., Pedersen, P.L., and Amzel, L.M. (1998). The 2.8-Å structure of rat liver F$_1$-ATPase: configuration of a critical intermediate in ATP synthesis/hydrolysis. Proc. Natl. Acad. Sci. USA *95*, 11065–11070.

Böttcher, B., Bertsche, I., Reuter, R., and Gräber, P. (2000). Direct visualisation of conformational changes in EF$_o$F$_1$ by electron microscopy. J. Mol. Biol. *296*, 449–457.

Boyer, P.D. (1997). The ATP synthase—a splendid molecular machine. Annu. Rev. Biochem. *66*, 717–749.

Braig, K., Menz, R.I., Montgomery, M.G., Leslie, A.G.W., and Walker, J.E. (2000). Structure of bovine mitochondrial F$_1$-ATPase inhibited by Mg^{2+}ADP and aluminium fluoride. Structure *8*, 567–573.

Brünger, A.T., Adams, P.D., Clore, G.M., DeLano, W.L., Gros, P., Grosse-Kunstleve, R.W., Jiang, J.S., Kuszewski, J., Nilges, M., Pannu, N.S., et al. (1998). Crystallography & NMR System: a new software suite for macromolecular structure determination. Acta Crystallogr. D Biol. Crystallogr. *54*, 905–921.

Cabezón, E., Montgomery, M.G., Leslie, A.G.W., and Walker, J.E. (2003). The structure of bovine F$_1$-ATPase in complex with its regulatory protein IF$_1$. Nat. Struct. Biol. *10*, 744–750.

Capaldi, R.A., and Aggeler, R. (2002). Mechanism of the F$_1$F$_o$-type ATP synthase, a biological rotary motor. Trends Biochem. Sci. *27*, 154–160.

CCP4 (Collaborative Computational Project, Number 4) (1994). The CCP4 suites: programs for protein crystallography. Acta Crystallogr. D Biol. Crystallogr. *50*, 760–763.

Cook, G.M., Keis, S., Morgan, H.W., von Ballmoos, C., Matthey, U., Kaim, G., and Dimroth, P. (2003). Purification and biochemical characterization of the F$_1$F$_o$-ATP synthase from thermoalkaliphilic *Bacillus* sp. strain TA2.A1. J. Bacteriol. *185*, 4442–4449.

DeLano, W.L. (2002). The PyMOL User's Manual (San Carlos, CA: DeLano Scientific).

Digel, J.G., Moore, N.D., and McCarty, R.E. (1998). Influence of divalent cations on nucleotide exchange and ATPase activity of chloroplast coupling factor 1. Biochemistry *37*, 17209–17215.

Dimroth, P., and Cook, G.M. (2004). Bacterial Na$^+$- or H$^+$-coupled ATP synthases operating at low electrochemical potential. Adv. Microb. Physiol. *49*, 175–218.

Dimroth, P., von Ballmoos, C., and Meier, T. (2006). Catalytic and mechanical cycles in F-ATP synthases. Fourth in the Cycles Review Series. EMBO Rep. *7*, 276–282.

Emsley, P., and Cowtan, K. (2004). Coot: model-building tools for molecular graphics. Acta Crystallogr. D Biol. Crystallogr. *60*, 2126–2132.

Feniouk, B.A., Suzuki, T., and Yoshida, M. (2006). The role of subunit ε in the catalysis and regulation of F$_o$F$_1$-ATP synthase. Biochim. Biophys. Acta *1757*, 326–338.

Gao, Y.Q., Yang, W., and Karplus, M. (2005). A structure-based model for the synthesis and hydrolysis of ATP by F$_1$-ATPase. Cell *123*, 195–205.

Gibbons, C., Montgomery, M.G., Leslie, A.G.W., and Walker, J.E. (2000). The structure of the central stalk in bovine F$_1$-ATPase at 2.4 Å resolution. Nat. Struct. Biol. *7*, 1055–1061.

Hanahan, D., Jessee, J., and Bloom, F.R. (1991). Plasmid transformation of *Escherichia coli* and other bacteria. Methods Enzymol. *204*, 63–113.

Hausrath, A.C., Grüber, G., Matthews, B.W., and Capaldi, R.A. (1999). Structural features of the γ subunit of the *Escherichia coli* F$_1$ ATPase revealed by a 4.4-Å resolution map obtained by X-ray crystallography. Proc. Natl. Acad. Sci. USA *96*, 13697–13702.

Hausrath, A.C., Capaldi, R.A., and Matthews, B.W. (2001). The conformation of the ε- and γ-subunits within the *Escherichia coli* F$_1$ ATPase. J. Biol. Chem. *276*, 47227–47232.

Hicks, D.B., and Krulwich, T.A. (1990). Purification and reconstitution of the F$_1$F$_o$-ATP synthase from alkaliphilic *Bacillus firmus* OF4. Evidence that the enzyme translocates H$^+$ but not Na$^+$. J. Biol. Chem. *265*, 20547–20554.

Ho, S.N., Hunt, H.D., Horton, R.M., Pullen, J.K., and Pease, L.R. (1989). Site-directed mutagenesis by overlap extension using the polymerase chain reaction. Gene *77*, 51–59.

Hoffmann, A., and Dimroth, P. (1990). The ATPase of *Bacillus alcalophilus*. Purification and properties of the enzyme. Eur. J. Biochem. *194*, 423–430.

Itoh, H., Takahashi, A., Adachi, K., Noji, H., Yasuda, R., Yoshida, M., and Kinosita, K., Jr. (2004). Mechanically driven ATP synthesis by F$_1$-ATPase. Nature *427*, 465–468.

Kabsch, W. (1993). Automatic processing of rotation diffraction data from crystals of initially unknown symmetry and cell constants. J. Appl. Cryst. *26*, 795–800.

Kagawa, R., Montgomery, M.G., Braig, K., Leslie, A.G.W., and Walker, J.E. (2004). The structure of bovine F$_1$-ATPase inhibited by ADP and beryllium fluoride. EMBO J. *23*, 2734–2744.

Keis, S., Kaim, G., Dimroth, P., and Cook, G.M. (2004). Cloning and molecular characterization of the *atp* operon encoding for the F$_1$F$_o$-ATP synthase from a thermoalkaliphilic *Bacillus* sp. strain TA2.A1. Biochim. Biophys. Acta *1676*, 112–117.

Keis, S., Stocker, A., Dimroth, P., and Cook, G.M. (2006). Inhibition of ATP hydrolysis by thermoalkaliphilic F$_1$F$_o$-ATP synthase is controlled by the C terminus of the ε subunit. J. Bacteriol. *188*, 3796–3804.

Lowry, D.S., and Frasch, W.D. (2005). Interactions between βD372 and γ subunit N-terminus residues γK9 and γS12 are important to catalytic activity catalyzed by *Escherichia coli* F$_1$F$_o$-ATP synthase. Biochemistry *44*, 7275–7281.

Ludtke, S.J., Baldwin, P.R., and Chiu, W. (1999). EMAN: semiautomated software for high-resolution single-particle reconstructions. J. Struct. Biol. *128*, 82–97.

McCoy, A.J., Grosse-Kunstleve, R.W., Storoni, L.C., and Read, R.J. (2005). Likelihood-enhanced fast translation functions. Acta Crystallogr. D Biol. Crystallogr. *61*, 458–464.

Mellwig, C., and Böttcher, B. (2003). A unique resting position of the ATP-synthase from chloroplasts. J. Biol. Chem. *278*, 18544–18549.

Menz, R.I., Walker, J.E., and Leslie, A.G.W. (2001). Structure of bovine mitochondrial F$_1$-ATPase with nucleotide bound to all three catalytic sites: implications for the mechanism of rotary catalysis. Cell *106*, 331–341.

Nalin, C.M., and McCarty, R.E. (1984). Role of a disulfide bond in the γ subunit in activation of the ATPase of chloroplast coupling factor 1. J. Biol. Chem. *259*, 7275–7280.

Noji, H., and Yoshida, M. (2001). The rotary machine in the cell, ATP synthase. J. Biol. Chem. *276*, 1665–1668.

Nowak, K.F., and McCarty, R.E. (2004). Regulatory role of the C-terminus of the ε subunit from the chloroplast ATP synthase. Biochemistry *43*, 3273–3279.

Nowak, K.F., Tabidze, V., and McCarty, R.E. (2002). The C-terminal domain of the ε subunit of the chloroplast ATP synthase is not required for ATP synthesis. Biochemistry *41*, 15130–15134.

Peng, G., Bostina, M., Radermacher, M., Rais, I., Karas, M., and Michel, H. (2006). Biochemical and electron microscopic characterization of the F$_1$F$_0$ ATP synthase from the hyperthermophilic eubacterium *Aquifex aeolicus*. FEBS Lett. *580*, 5934–5940.

Pettersen, E.F., Goddard, T.D., Huang, C.C., Couch, G.S., Greenblatt, D.M., Meng, E.C., and Ferrin, T.E. (2004). UCSF Chimera—a visualization system for exploratory research and analysis. J. Comput. Chem. *25*, 1605–1612.

Richter, M.L., Patrie, W.J., and McCarty, R.E. (1984). Preparation of the ε subunit and ε subunit-deficient chloroplast coupling factor 1 in reconstitutively active forms. J. Biol. Chem. *259*, 7371–7373.

Rodgers, A.J.W., and Wilce, M.C.J. (2000). Structure of the γ-ε complex of ATP synthase. Nat. Struct. Biol. *7*, 1051–1054.

Rubinstein, J.L., Walker, J.E., and Henderson, R. (2003). Structure of the mitochondrial ATP synthase by electron cryomicroscopy. EMBO J. *22*, 6182–6192.

Schägger, H., Aquila, H., and von Jagow, G. (1988). Coomassie blue-sodium dodecyl sulfate-polyacrylamide gel electrophoresis for direct visualization of polypeptides during electrophoresis. Anal. Biochem. *173*, 201–205.

Shirakihara, Y., Leslie, A.G.W., Abrahams, J.P., Walker, J.E., Ueda, T., Sekimoto, Y., Kambara, M., Saika, K., Kagawa, Y., and Yoshida, M. (1997). The crystal structure of the nucleotide-free α$_3$β$_3$ subcomplex of F$_1$-ATPase from the thermophilic *Bacillus* PS3 is a symmetric trimer. Structure *5*, 825–836.

Stock, D., Leslie, A.G.W., and Walker, J.E. (1999). Molecular architecture of the rotary motor in ATP synthase. Science *286*, 1700–1705.

Stocker, A., Keis, S., Cook, G.M., and Dimroth, P. (2005). Purification, crystallization, and properties of F$_1$-ATPase complexes from the thermoalkaliphilic *Bacillus* sp. strain TA2.A1. J. Struct. Biol. *152*, 140–145.

Tsunoda, S.P., Rodgers, A.J.W., Aggeler, R., Wilce, M.C.J., Yoshida, M., and Capaldi, R.A. (2001). Large conformational changes of the ε subunit in the bacterial F$_1$F$_0$ ATP synthase provide a ratchet action to regulate this rotary motor enzyme. Proc. Natl. Acad. Sci. USA *98*, 6560–6564.

van Heel, M., Harauz, G., Orlova, E.V., Schmidt, R., and Schatz, M. (1996). A new generation of the IMAGIC image processing system. J. Struct. Biol. *116*, 17–24.

Winn, M.D., Isupov, M.N., and Murshudov, G.N. (2001). Use of TLS parameters to model anisotropic displacements in macromolecular refinement. Acta Crystallogr. D Biol. Crystallogr. *57*, 122–133.

Xing, J., Liao, J.-C., and Oster, G. (2005). Making ATP. Proc. Natl. Acad. Sci. USA *102*, 16539–16546.

Yasuda, R., Noji, H., Yoshida, M., Kinosita, K., Jr., and Itoh, H. (2001). Resolution of distinct rotational substeps by submillisecond kinetic analysis of F$_1$-ATPase. Nature *410*, 898–904.

Zimmermann, B., Diez, M., Zarrabi, N., Graber, P., and Borsch, M. (2005). Movements of the ε-subunit during catalysis and activation in single membrane-bound H$^+$-ATP synthase. EMBO J. *24*, 2053–2063.

Accession Numbers

The structure of thermoalkaliphilic F$_1$-ATPase has been deposited in the Protein Data Bank under ID code 2QE7.